PCCP

PAPER

View Article Online
View Journal

Check for updates

Cite this: DOI: 10.1039/d6cp00071a

Dual-enhanced fluorescent biosensors using metal-coated piezoelectric nanoimprinted substrates

Ghadeer Almohammadi, [ab] Dominik Duleba, [a] Aeshah F. Alotaibi, [cd] Eni Kume, [d] Adrià Martinez-Aviñó, [a] James H. Rice *[d] and Robert P. Johnson *[a]

Received 8th January 2026,
Accepted 26th March 2026

DOI: 10.1039/d6cp00071a

rsc.li/pccp

The integration of piezoelectric polymers with metallic nanostructures provides new opportunities for developing highly responsive fluorescent sensing devices. In this work, we show that nanoimprinted poly(vinylidene fluoride) thin films coated with a thin gold layer can amplify the fluorescence signal of Cy3-labelled DNA and improve detection sensitivity. Signal enhancement is assigned to both the surface plasmon resonance of the nanofeatures as well as to the piezoelectric-based enhancement of fluorescence when a mechanical pressure is applied to the substrate. Our study also reveals that moderate mechanical force maximises the piezoelectricity-based enhancement, while larger forces degrade the substrate. This highly sensitive platform was shown to possess good selectivity as evaluated through exposure to non-complementary sequences, as well as good reusability through ozone UV cleaning. The work highlights the potential of hybrid metal-coated and nanoimprinted piezoelectric substrates as a promising platform for highly sensitive and selective biosensors.

Open Access Article. Published on 26 March 2026. Downloaded on 4/16/2026 1:26:30 AM.
This article is licensed under a Creative Commons Attribution 3.0 Unported Licence.

Introduction

The development of reliable and highly sensitive biosensors remains an essential challenge in medical diagnostics, food safety, and environmental monitoring.[1,2] DNA-based biosensors, which detect analytes through interactions with aptamers,[3] DNAzymes,[4] or DNA probes,[5] have attracted particular attention.[6] Compared to enzyme or antibody-based alternatives, they offer high thermal tolerance,[7] easy modification,[8] efficient surface regeneration,[6] and greater resistance to enzymatic degradation in complex biological and environmental matrices.[9] Additionally, DNA probes for various targets can be readily obtained through directed screening of DNA libraries,[10] making these biosensors readily adaptable.[5]

Among DNA-based biosensors, those that rely on fluorescence-based signal transduction are widespread due to their rapid response times,[11] high suitability for complex biological and environmental matrices,[12] and multiplexing capacity.[13] While they have been widely utilised to develop robust, cost-effective, and easy-to-use biosensors,[14] new strategies are constantly being explored to improve their sensitivity by amplifying the fluorescence signal.[13]

One approach to amplifying the response of fluorescence-based DNA biosensors is to tune the supporting substrate to enable or maximise surface-enhaced fluorescence. Nanostructured metallic substrates can interact with light and produce localised surface plasmons, leading to surface-enhanced fluorescence (SEF),[15,16] while piezoelectric substrates can generate a piezoelectric potential to further enhance the fluorescence intensity.[17] Poly(vinylidene fluoride) (PVDF) is particularly promising in this context as it is a semicrystalline polymer whose β-phase is an all-trans planar zigzag chain conformation, which aligns the molecular dipoles, resulting in piezoelectric activity.[18] The piezoelectric performance is strongly linked to the fraction of the polar β-phase, which is sensitive to processing and post-treatment conditions.[19,20] Common strategies to increase β-phase content include electrospinning or solution blow-spinning to produce nanofibers, mechanical stretching of cast films, and annealing at elevated temperatures to promote a conformational transition from the α-phase to the β-phase.[19,21] These approaches can yield PVDF with very high β-phase fractions and enhanced piezoelectric coefficients, particularly in nanofibrous architectures.[15,16,21]

While piezoelectric substrates can generate a piezoelectric potential to further enhance the fluorescence intensity,[17] poly(vinylidene fluoride) (PVDF) is particularly promising in this context as PVDF not only has desirable piezoelectric properties, but it can be easily processed and nanoimprinted with features, followed by the application of a metallic coating to make it exhibit localised surface plasmon resonance.[22] Our groups have previously demonstrated that gold-coated nanohole-imprinted PVDF enhanced the fluorescence intensity of quantum dots,

[a] School of Chemistry, University College Dublin, Belfield, D04 V1W8, Ireland. E-mail: robert.johnson@ucd.ie
[b] Department of Chemistry, College of Science, University of Hafr Al-Batin, Hafr Al-Batin, Saudi Arabia
[c] School of Physics, University College Dublin, Belfield, D04 V1W8, Ireland
[d] Department of Physics, College of Science and Humanities, Shaqra University, Shaqra, 11961, Kingdom of Saudi Arabia. E-mail: james.rice@ucd.ie

Open Access Article. Published on 26 March 2026. Downloaded on 4/16/2026 1:26:30 AM.
This article is licensed under a Creative Commons Attribution 3.0 Unported Licence.

and that this fluorescence intensity could be controllably further amplified through the piezoelectric effect of the substrate, which was controlled *via* the application of mechanical pressure.[17]

Systematic studies of DNA sensing using nanoimprinted piezoelectric substrates are limited. Earlier works have predominantly focused on nanostructures fabricated on rigid supports, and flexible piezoelectric polymers, such as PVDF, have been less explored. Recent work on nanoimprinted PVDF-HFP films combined with metallic nanostructures has demonstrated piezoelectric-driven amplification of plasmon-enhanced fluorescence, where an applied mechanical load generated a piezoelectric potential that increases the local electric field and enhances the emission of quantum dots and DNA hybridisation assays on gold-coated substrates.[17] In addition, electro-spun PVDF and PVDF-based nanocomposites have shown simultaneous improvements in piezoelectric response and fluorescence, attributed to strain-induced internal fields and a higher fraction of polar crystalline phases that modulate radiative recombination.[23] Strain-dependent optical studies on individual ZnO nanorods further support this concept, revealing that bending-induced piezoelectric polarisation can tune fluorophore emission *via* the piezo-phototronic effect.[24,25] Together, these reports indicate that both PVDF-based polymers and inorganic piezoelectric materials can act as active substrates where mechanically generated piezoelectric potentials are exploited to control fluorescence intensity in sensing and related optical applications.[2]

Herein, we build on our previous work and use a different nanoimprinted substrate, a nano trench-imprinted gold-coated PVDF,[17,26] to develop a model fluorescent DNA biosensor which exploits both surface-plasmon- and piezoelectric-enhanced fluorescence. We explore the influence of complementary target DNA concentration and the applied mass on the signal enhancement, showing that the limits of detection are improved by both the nanostructured substrate and the piezoelectric effect of the underlying PVDF support. We also demonstrate sensor reusability through regeneration with an ozone UV cleaning method, as well as sensor specificity through exposure to non-complementary target DNA. This work establishes a dual-amplification DNA-based fluorescence platform which can be readily adapted to diverse targets and builds the foundations towards ultrasensitive fluorescent point-of-care diagnostic and field-deployable sensors.

Experimental

Materials and reagents

Poly(vinylidene fluoride) (PVDF) powder (average molecular weight ≈ 534 000), *N*-dimethylformamide (DMF, ≥99.8%), ethanol (EtOH), and phosphate-buffered saline (PBS, pH 7.4) were purchased from Sigma-Aldrich and used without further purification. Gold coatings were prepared using an EMITECH K575X evaporation system. All aqueous solutions were prepared using Milli-Q water (18.2 MΩ cm).

Substrate fabrication and gold-coated nanoimprinted PVDF film

A 20 wt/vol% solution of PVDF was prepared by dissolving 1 g of PVDF powder in 5 mL of DMF and stirring at 60–70 °C for 2 h. This solution was spin-casted (home-built spin coater at 1 V for 30 s) onto a glass cover slip to prepare the flat PVDF substrates (Fig. 1A), or onto a nanotrench-imprinted silicon stamp purchased from II–VI Aerospace & Defense (110 nm depth, 417 nm period) to prepare the nanotrench-imprinted PVDF film (Fig. 1B). Following

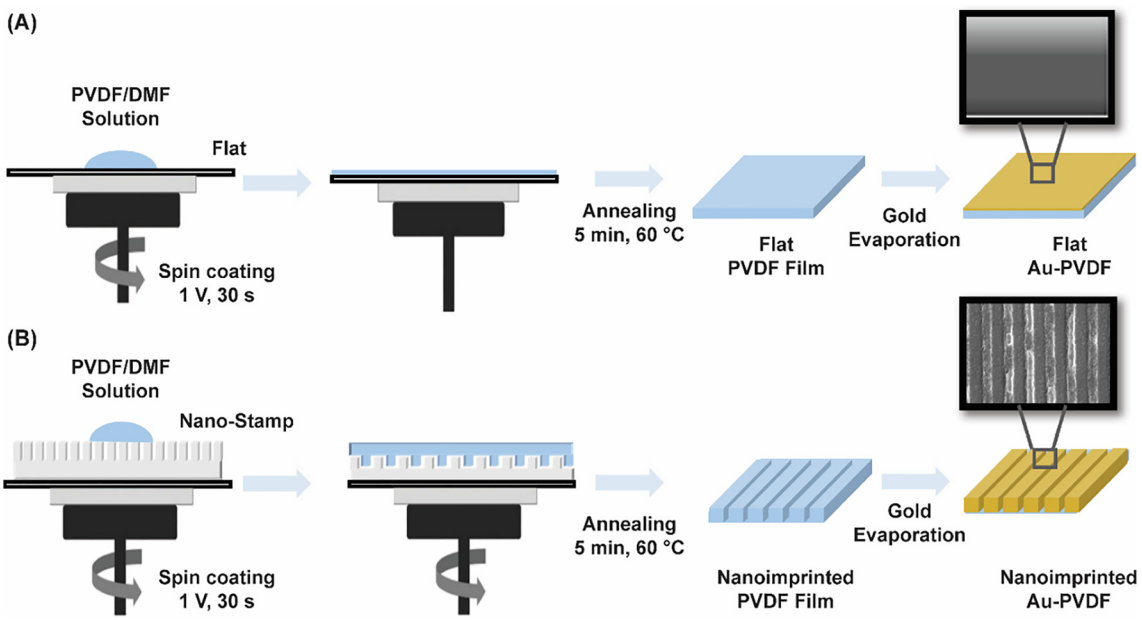

Fig. 1 shows the preparation of the (A) flat and (B) nanoimprinted PVDF films. Both films are prepared by spin-coating a PVDF solution onto a silicon mould (flat or nanoimprinted), followed by drying, annealing, and gold layer deposition.

This journal is © the Owner Societies 2026

Open Access Article. Published on 26 March 2026. Downloaded on 4/16/2026 1:26:30 AM.
This article is licensed under a Creative Commons Attribution 3.0 Unported Licence.

spin casting, a PVDF film thickness of 5.5 μm was obtained, as measured by Sycon Instruments STM-100/MF thickness monitor (4 kW). The solution was then annealed at 60 °C for 5 min to stabilise the film morphology and promote β-phase formation while avoiding deformation or relaxation of the nanoimprinted features. The substrate was gently peeled off to preserve the imparted morphology and then was subjected to gold-coating by thermal evaporation at 2 nm s^{-1} for 30 s. Gold coating produced a nominal gold thickness of approximately 10 nm; no additional adhesion layer was used. Surface morphology and nanoscale features were examined with atomic force microscopy (AFM, Bruker Dimension Icon). Fourier-transform infrared (FTIR) spectroscopy (Bruker Tensor 27) was used to identify the crystalline phases of PVDF films. Reflectance spectra were collected with an Agilent Cary 5000 UV-vis spectrophotometer in the wavelength range of 300–800 nm. Contact angle measurements were performed using a Krüss DSA25, and the average contact angles of at least three drops per substrate were reported. Electrochemical measurements were used to determine substrate surface area (Fig. S1), where the cyclic voltammetry of 1 mM ruthenium(III) hexamine was recorded at the substrate using a BioLogic SP-200 potentiostat.

Piezoelectric characterisation

Open-circuit voltage was measured using an Agilent Technologies DSO1052B Digital Storage Oscilloscope (50 MHz, 1 GSa s^{-1}). Samples were contacted with electrodes and subjected to rapid mechanical tapping using a pen to induce dynamic loading/unloading cycles. Voltage transients were recorded in fast acquisition mode over multiple cycles for both flat and nanoimprinted Au-coated PVDF substrates.

Immobilization and hybridization of the DNA

All synthetic DNA sequences were purchased from Biomers.net GmBH and reconstituted in 10 mM PBS (pH 7). The probe sequence was designed complementary to a short sequence found in the housekeeping gapA gene of *Klebsiella Pneumoniae* with the addition of a thiol-modification at the 3′ end (TGT GTT TAC GAG CGG TTT CG/3ThioMC3-D). The fully complementary target sequence for this model system was labelled at the 5′ end with the commercial dye Cy-3 (Cy-3/CGA AAC CGC TCG TAA ACA CA). A synthetic target from the bacterium *Shigella Flexineri* (Cy-3/5′-CCT TTT CCG CGT TCC TTG A-3′) was used as the non-complementary target.

Probe immobilisation

A stock solution of 10 μM thiolated probe DNA was prepared in 10 mM PBS (pH 7). Probe immobilisation was carried out by incubating the gold-coated PVDF substrates with a solution containing 1 μM probe DNA and 10 μM mercaptohexanol (MCH) prepared in 10 mM PBS (pH 7). The substrates were left to incubate at room temperature for 16 h to allow the thiolated probes to bind to the gold surface. Following immobilisation, the substrates were thoroughly rinsed with PBS to remove unbound DNA and dried under a gentle stream of nitrogen.

Following probe immobilization, substrates were exposed to a 10 μM target DNA in 10 mM PBS (pH 7). The substrates were briefly heated to 90 °C for 2 min and cooled for 1 h to promote hybridisation, followed by washing with PBS and drying under nitrogen.

Fluorescence intensity measurements

Fluorescence spectra were acquired using a Horiba Scientific spectrofluorometer with 532 nm excitation (1 mW laser power), 1 s integration time, and 10 accumulations per spectrum. Data were smoothed using FFT filter (50% cutoff) to suppress high-frequency noise while preserving peak shape. Reported intensities represent the mean ± standard error of the mean (SEM) from $n = 20$.[27] The 532 nm diode laser was linearly polarised, but the sample orientation relative to the grating vector was not actively controlled, resulting in a fixed, uncontrolled polarisation condition for all measurements. The excitation wavelength corresponds to the UV-vis absorption of the fluorescent label (Fig. S2). For fluorescence measurements, the substrates were sandwiched between two glass cover slips, with the nanoimprinted surface pointing downwards towards the excitation laser, allowing a weight to be placed on the top cover slip. Piezoelectric fluorescence measurements were performed by placing the specified weight on the top cover slip and waiting 5 s for stabilisation before spectral acquisition. Time-dependent fluorescence measurements show that this measurement time is within the transient piezoelectric response. (Fig. S3) All fluorescence measurements were collected from up to twenty different 10 μm spots on each substrate to minimize the impact of trench-to-trench inhomogeneities (Fig. S4).

Finite element simulations

Finite element analysis was carried out using the Electromagnetic Waves module in COMSOL Multiphysics. A 2D representation of two periodic unit cells of the imprinted surface was used to propagate the electromagnetic waves. The refractive indices are taken as 1.4 + i0.02 for PVDF, while the refractive indices of Au are taken from Rosenblatt *et al.*,[28] An incident beam perpendicular to the sample surface and polarized to the *x*-axis is considered. This *x*-polarisation corresponds to optimal coupling with the grating vector and represents an upper bound on the plasmonic field enhancement achievable under polarisation-matched conditions. Perfectly Matched Layers (PML) are used to surround the unit cell to prevent back-reflected waves. The enhancement factor is calculated from the electric field enhancement around the surface of the nanostructures:[29]

$$\mathrm{EF} = \frac{|E|^2}{|E_0|^2}\frac{\gamma_\mathrm{r}}{\gamma_\mathrm{nr} + \gamma_\mathrm{r}}$$

where E is the electric field that is locally enhanced on the quantum dot surface, E_0 is the background electric field, and γ_r and γ_nr are the radiative and thermal dissipated nonradiative powers. For the calculations of the radiative and thermal dissipated nonradiative powers, an electric point dipole was placed near the surface. The surface integral of the time-averaged

Open Access Article. Published on 26 March 2026. Downloaded on 4/16/2026 1:26:30 AM.
This article is licensed under a Creative Commons Attribution 3.0 Unported Licence.

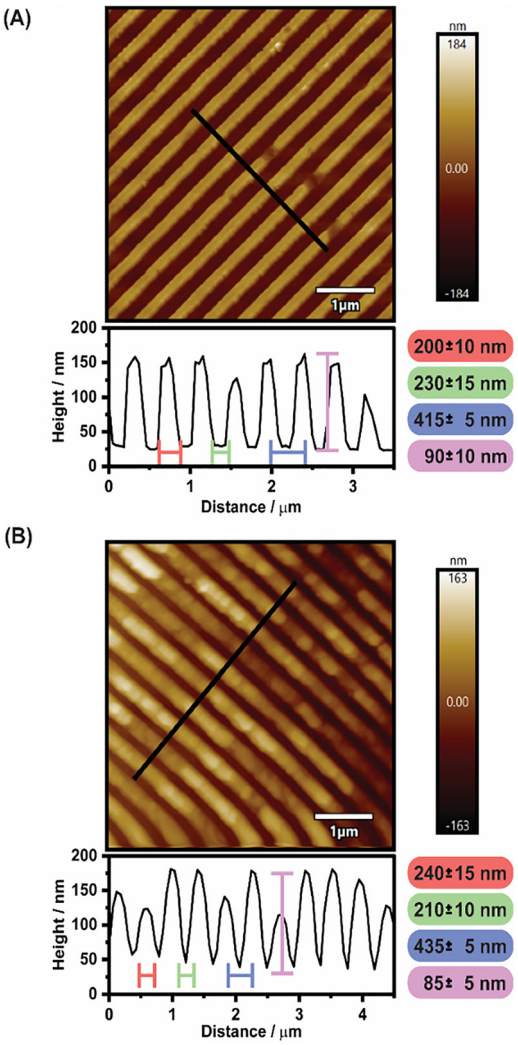

Fig. 2 shows the AFM images and profile plots of nanoimprinted PVDF (A) before and after (B) gold-coating. The figure shows that the nanofeatures are preserved with some changes to the nanofeature dimension corresponding to the deposited gold layer.

Poynting vector around the quantum dot gave the radiative losses, while the volume integral of the total power dissipation density on the nearby surface provided the thermal losses. To represent the generated piezoelectric potential from the application of a load, a surface current density is used on the surface. This effectively interacts with the propagation of the incident beam.

Reusability studies

To evaluate substrate reusability, probe-functionalized samples were subjected to ozone UV cleaning for 40 min. After cleaning, the substrates were immediately washed with Milli-Q water, rinsed with ethanol, and dried under a gentle stream of nitrogen. The efficiency of DNA removal and the preservation of the nanostructures were confirmed by fluorescence spectroscopy and AFM imaging.

Results and discussion

Nanotrench-imprinted gold-coated PVDF substrates were prepared by spin coating a PVDF solution onto a nanoimprinted silicon stamp, followed by annealing, and gold layer deposition. Fig. 2A shows an AFM image of the nanoimprinted PVDF substrate prior to gold coating, revealing well-defined periodic nanotrenches with an average periodicity of 415 ± 5 nm, a groove depth of 90 ± 10 nm, and a line width of 230 ± 15 nm. Following the deposition of a thin gold layer, the nanoscale features are retained with an increased periodicity of 435 ± 5 nm, decreased groove depth of 85 ± 5 nm, and decreased line width of 210 ± 10 nm. (Fig. 2B) This indicates that a thin layer of gold (*circa* 10 nm) is deposited, and conforms to the underlying nanostructure, retaining the overall nanoimprinted geometry.

The preparation and processing route of the PVDF substrates is known to strongly influence the fraction of the β-phase,[18,30] and hence the piezoelectric activity and potential signal amplification in biosensing applications. Herein, we focus on spin-coated PVDF films compatible with nanoimprint lithography and use a mild annealing step that stabilises the film and promotes β-phase formation while preserving the imprinted trench morphology.[19]

The fraction of the β-phase was evaluated using the characteristic FTIR absorption bands associated with the α- and β-phases of PVDF at wavelengths of 770 cm^{-1} and 836 cm^{-1}, respectively (Fig. S5A). The flat films exhibited a β-phase fraction of 76.2 ± 3.6%, while the nanoimprinted films showed 74.1 ± 4.5%. These values are in agreement with a previous report of 72% in PVDF films prepared at 20 wt%.[18] Slight deviations in the β-phase can be attributed to differences in processing conditions, film thickness, or solvent evaporation rates.[18] More aggressive β-phase preparation protocols yielding higher β-phase contents may be beneficial for maximising piezoelectric response; however, retaining the nanoimprinted features is critical.

Reflectance spectra (Fig. S5B) were used to compare the optical behaviour of flat and nanoimprinted substrates. The reflectance spectra show that flat Au–PVDF has characteristic gold interband absorption in the 450–550 nm range, while the nanoimprinted substrates exhibit stronger wavelength-dependent modulation consistent with grating-coupled plasmonic effects. This behaviour demonstrates that nanostructuring can modulate light–matter interactions at the surface, which is expected to influence fluorescence efficiency.

The gold-coated nanoimprinted PVDF substrates were subsequently modified with thiolated DNA probes using gold–thiol chemistry, resulting in a biosensor that is responsive to complementary target DNA due to a specific hybridisation reaction that immobilises the fluorescence probe. (Fig. 3A) The functionalization and hybridisation steps were experimentally confirmed by contact angle measurements, which showed a decrease in hydrophobicity (decreasing contact angle) as the probe and target were immobilised, consistent with the immobilisation of the charged and hydrophilic negatively charged phosphate groups. (Fig. 3B) Fluorescence spectroscopy was also

This journal is © the Owner Societies 2026

Open Access Article. Published on 26 March 2026. Downloaded on 4/16/2026 1:26:30 AM.
This article is licensed under a Creative Commons Attribution 3.0 Unported Licence.

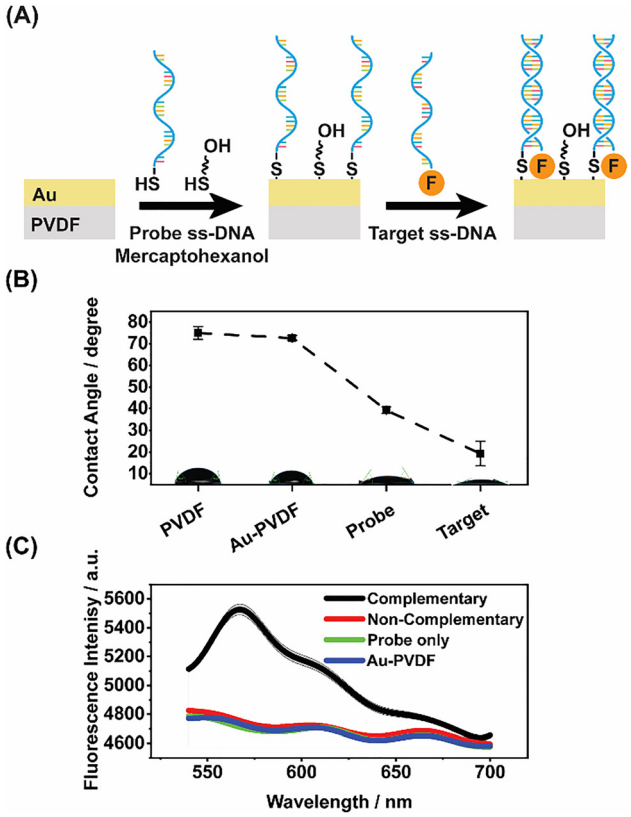

Fig. 3 shows (A) a schematic of the probe DNA functionalisation process on the Au-coated PVDF substrate, followed by the probe immobilisation. (B) The contact angle measurements of bare PVDF, Au-coated PVDF, probe DNA, and target DNA modified Au–PVDF surfaces are also shown, verifying the successful immobilization of DNA onto the substrate. Error bars represent the standard error calculated from three drops measured on each substrate. (C) The fluorescence spectrum associated with each modification step is also shown, further verifying the successful and specific hybridization of the Cy3-labelled GapA target DNA. A 532 nm excitation wavelength is used. The shaded area represents the standard error from 20 different measurements at different spots on the same substrate.

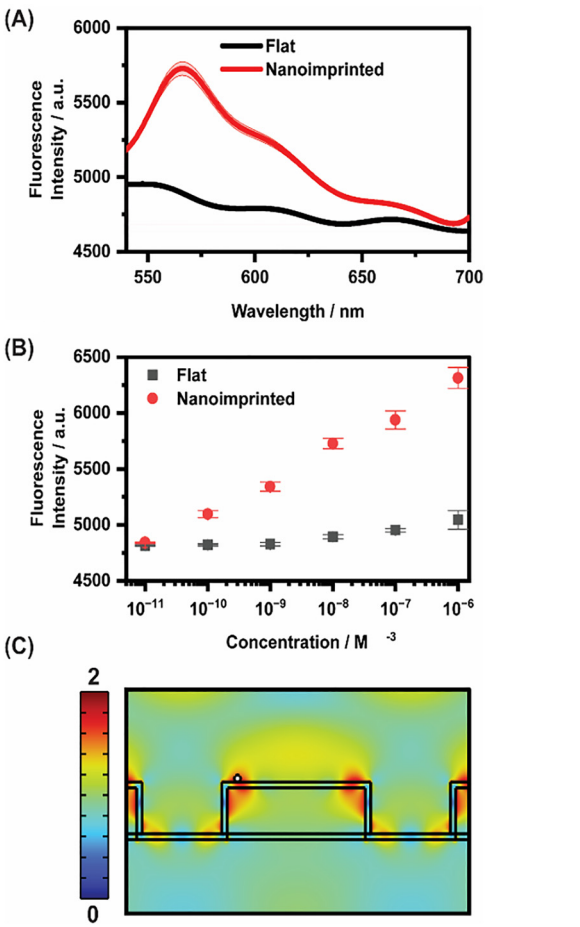

Fig. 4 shows the (A) fluorescence spectra of flat and nanoimprinted Au–PVDF, (B) the fluorescence intensities as a function of target DNA concentration, and (C) a finite element simulation of the electric field enhancement around the nanoimprinted features. Error bars represent the standard error of at least 20 replicate measurements carried out on the same substrate at different measurement spots.

used to verify the binding of the Cy3-labelled target DNA, as well as the specificity of the hybridisation reaction with the probe. Fig. 3C shows a significant increase in the fluorescence intensity upon the immobilisation of the target DNA, while a non-complementary Cy3-labelled DNA showed no change in fluorescence intensity. This verifies both the successful hybridisation of the target DNA, as well as the specificity of the sensor.

The potential for reusing the functionalised substrates was investigated using ozone UV cleaning as a regeneration method. Fig. S6 shows that the fluorescence peak of 10 μM target can be removed using an ozone UV clean, and then re-attachment of the probe DNA and re-exposure to the target recovers the fluorescence intensity to a level comparable with the original signal. AFM was used to assess the effect of the cleaning treatment on the substrate morphology, revealing that even following cleaning, the same nanoscale features are retained with no visible damage. (Fig. S7) The height–distance profiles confirm that the periodicity and groove depth were preserved after treatment. (Fig. S7) These results demonstrate that ozone UV cleaning effectively removes DNA molecules without altering the nanoscale architecture of the substrate, providing a reliable regeneration strategy for repeated biosensing applications.

Dual-amplification of fluorescence signal

To evaluate the dual-amplification action of the gold-coated nanoimprinted PVDF substrates, their fluorescence response as a function of target DNA concentration is compared to that of the gold-coated flat PVDF substrate. Fig. 4A shows the fluorescence response of the flat and nanoimprinted substrates in the absence of a mechanically applied pressure (no piezoelectric effect). Fig. 4B shows that the nanoimprinted substrate exhibits higher fluorescence intensities and lower limits of detection compared to the flat substrate. (LOD_{flat} = 2000 pM and $LOD_{imprint}$ = 8 pM) Limits of detection are calculated by fitting a linear-log equation ($y = a - b \ln x$) to the calibration data and interpolating the

Open Access Article. Published on 26 March 2026. Downloaded on 4/16/2026 1:26:30 AM.
This article is licensed under a Creative Commons Attribution 3.0 Unported Licence.

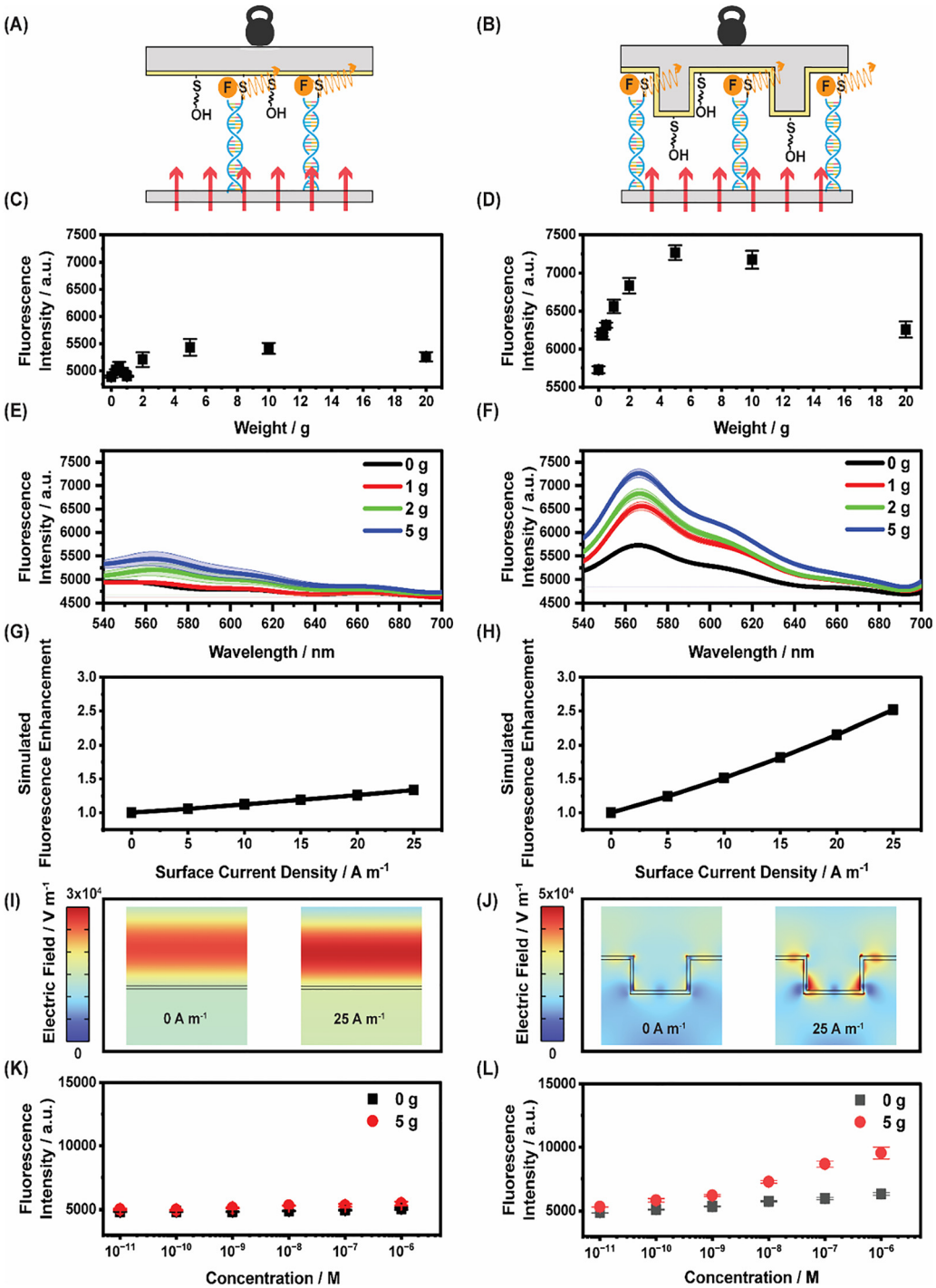

Fig. 5 (A) and (B) show the fluorescence measurement setup and how the piezoelectric material is activated by the applied weight on both the flat and nanoimprinted substrates. Fluorescence intensity of (C) flat and (D) nanoimprinted Au-coated PVDF substrate under different applied weights (0.3–20 g) with 10^{-9} M of target DNA is shown. The fluorescence spectra (E) and (F) corresponding to different applied weights are also provided. (G) and (H) shows the simulated fluorescence enhancement values relative to the non-pressed state. (I) and (J) shows the changes to the electric field strength when a surface current density is applied. (K) and (L) shows concentration-dependent fluorescence response of flat and nanoimprinted substrate in the non-pressed and pressed (5 g weight) states. Error bars represent the standard error of at least 20 replicate measurements carried out on the same substrate at different measurement spots. The fluorescence spectrum for each concentration is provided in Fig. S9.

concentration value that produced a response of $3.3\sigma + \mu_{blank}$. The standard deviation (σ) is obtained through the fitting residuals of the lowest concentration data to avoid underestimation of the variance through blank measurements.

As shown in Fig. 4C, this signal amplification is partly a consequence of the localised surface plasmon resonance associated with the gratings of the gold-coated nanoimprinted substrates, where nanostructuring concentrates the electromagnetic field at

This journal is © the Owner Societies 2026

Open Access Article. Published on 26 March 2026. Downloaded on 4/16/2026 1:26:30 AM. This article is licensed under a Creative Commons Attribution 3.0 Unported Licence.

protrusions and edges, further enhancing the fluorescence from molecules located in these regions, as reported for nanostructured and roughened plasmonic electrodes.[15,31] Based on the enhancement of the electric field intensities, a 2.4-fold plasmon-based fluorescence emission enhancement is expected from the nanoimprinted substrate compared to the flat substrate.

The signal amplification is also associated with the increased geometric surface area and the three-dimensional curvature, which provide more available binding sites per projected area and can alleviate steric crowding between neighbouring DNA strands.[32] This facilitates denser yet accessible probe monolayers, leading to more Cy3-labelled duplexes within the excitation volume, and consequently higher fluorescence intensities.[32] Cyclic voltammetry was used to determine the surface coverage of the probe molecules, showing a higher surface coverage for the nanoimprinted substrate (7.70×10^{15} molecules cm^{-2}) than for the flat substrate (4.22×10^{14} molecules cm^{-2}). (Fig. S1) This translates into an 18-fold increase in the number of molecules excited within the 10 μm fluorescence excitation laser spot size.

To evaluate the influence of the PVDF's piezoelectric activity on the fluorescence response, the performance of flat and nanoimprinted gold-coated PVDF substrates was investigated under different applied weights at a fixed 1 nM target concentration. For piezoelectric-enhanced fluorescence measurements, the substrate is sandwiched between two glass plates, and a weight is applied on top (Fig. 5A and B). Fig. 5C and D shows that for the flat Au–PVDF substrate, the fluorescence signal increased steadily as the applied weight was raised from 0.3 g to 5 g, reaching a maximum intensity at 5 g. Beyond this point, the signal began to plateau and eventually declined at higher weights ($\geq$10 g), likely due to the decomposition of the substrate under the applied pressure and loss of piezoelectric activity near the excitation spot. A similar trend was observed for the nanoimprinted gold-coated PVDF substrate (Fig. 5D and F), where the optimal pressing condition was also found to be 5 g, however, fluorescence intensities were much higher. These results suggest that a moderate applied weight on a PVDF substrate can enhance fluorescence efficiency, aligning with the principle of piezoelectric-mediated signal amplification.[25] While the β-phase content of the flat and nanoimprinted substrates is similar, open circuit measurements show that the nanoimprinted substrate has slightly higher piezoelectric activity, likely due to the generation of higher stresses within the nanoimprinted structure. (Fig. S8) As such, the observed improvements in fluorescence are attributed to an enhanced coupling between favourable mechanical deformation, piezoelectric-induced surface charge redistribution, and nanostructure-assisted plasmonic field enhancement.

Finite element simulations were used to model the fluorescence enhancement arising from the piezoelectric effect. (Fig. 5G–J) The piezoelectric effect is modelled by applying a surface current density to the gold surface. A higher applied mass corresponds to higher stresses within the PVDF, which will polarise the piezoelectric material and impart surface charge density. As the surface charge relaxes, the changing surface charge will generate a surface current density. Correspondingly, higher applied loads can be qualitatively approximated by a higher surface current density. Fig. 5G–J shows the simulated fluorescence enhancement as the surface current density is increased. Both the increasing fluorescence enhancements, as well as the higher enhancements observed for the nanoimprinted surface, are qualitatively reproduced.

The sensitivity enhancement of the dual-amplification approach was evaluated through concentration-dependent fluorescence studies, where the optimum weight of 5 g was used to impose piezoelectric-enhanced fluorescence. Fig. 5K and L shows that on both the flat and nanoimprinted substrates, the piezoelectric effect can enhance the fluorescence signal and improve the limits of detection; however, the greatest signal improvement is observed on the nanoimprinted substrates, where the surface plasmon- and piezoelectric enhancements can work in tandem. The limit of detection of the flat substrate improves from 2000 pM to 40 pM, while the limit of detection of the nanoimprinted substrate improves from 8 pM to 0.9 pM upon piezoelectric enhancement. These results highlight that combining nanoscale surface features and mechanical pressure-induced piezoelectric enhancement synergistically enhances signal strength and biosensing sensitivity.

Conclusions

To conclude, this study demonstrated the dual-amplification potential of gold-coated nanoimprinted PVDF substrates. Due to the grating-like nanotrench features of the substrate, the localised surface plasmon resonance, the higher surface areas, and probe loadings amplified the fluorescence response and improved the limit of detection for *GapA* DNA from 2000 pM to 40 pM. The application of mechanical pressure was shown to further enhance the fluorescence response, with moderate applied forces (5 g) being optimal, while greater forces can be detrimental due to substrate breakdown. When the piezoelectric enhancement acts in tandem with the nanofeature-based enhancement, the greatest improvement in the limit of detection was observed, reaching as low as 0.9 pM. We also demonstrated that the substrate is robust and can be readily regenerated and reused without a significant loss of performance or the degradation of nanofeatures. Overall, these findings highlight the dual-amplifying nature of nanoimprinted gold-coated PVDF, establishing them as sensitive, specific, and reusable platforms for DNA biosensing applications.

Author contributions

GA: data curation, formal analysis, investigation, methodology, visualisation, writing (original draft). DD: formal analysis, investigation, methodology, visualisation, writing (original draft). AFA: investigation, writing (review & editing). EK: methodology, writing (review & editing). AMA: supervision, writing (review & editing). JHR: conceptualisation, methodology, funding acquisition, supervision, writing (review & editing). RPJ: conceptualisation, methodology, funding acquisition, supervision, writing (review & editing).

Open Access Article. Published on 26 March 2026. Downloaded on 4/16/2026 1:26:30 AM. This article is licensed under a Creative Commons Attribution 3.0 Unported Licence.

Conflicts of interest

There are no conflicts to declare.

Data availability

All data supporting the findings of this study are available within the article and its supplementary information (SI). Supplementary information is available. See DOI: https://doi.org/10.1039/d6cp00071a.

Acknowledgements

We acknowledge funding from Science Foundation Ireland under the Frontiers for the Future Programme (20/FFP-P/8728 and 21/FFP-P/10217). DD acknowledges postgraduate scholarship funding from the Irish Research Council (Project No. GOIPG/2022/1648). GA acknowledges postgraduate scholarship funding from the Ministry of Education in the Kingdom of Saudi Arabia, Hafr Al Batin University and the Saudi Arabian Cultural Mission.

Notes and references

1 B. Van Dorst, J. Mehta, K. Bekaert, E. Rouah-Martin, W. De Coen, P. Dubruel, R. Blust and J. Robbens, Recent advances in recognition elements of food and environmental biosensors: A review, *Biosens. Bioelectron.*, 2010, **26**(4), 1178–1194, DOI: 10.1016/j.bios.2010.07.033; A. M. Elbasiony, S. Alharthi, M. Mohamady Ghobashy, W. E. Boraie, M. S. Attia, M. Madani, S. Ali Al-Gahtany, R. Darwesh, M. Shaban and A. I. Sharshir, Development and application of novel biosensors for enhanced detection in medical diagnostics, *Microchem. J.*, 2024, **207**, 111938, DOI: 10.1016/j.microc.2024.111938.

2 R. M. Al-Shammari, M. A. Baghban, N. Al-attar, A. Gowen, K. Gallo, J. H. Rice and B. J. Rodriguez, Photoinduced Enhanced Raman from Lithium Niobate on Insulator Template, *ACS Appl. Mater. Interfaces*, 2018, **10**(36), 30871–30878, DOI: 10.1021/acsami.8b10076.

3 R. E. Wang, Y. Zhang, J. Cai, W. Cai and T. Gao, Aptamer-based fluorescent biosensors, *Curr Med Chem*, 2011, **18**(27), 4175–4184, DOI: 10.2174/092986711797189637 From NLMM. Muhammad and Q. Huang, A review of aptamer-based SERS biosensors: Design strategies and applications, *Talanta*, 2021, **227**, 122188, DOI: 10.1016/j.talanta.2021.122188; L. R. Paborsky, S. N. McCurdy, L. C. Griffin, J. J. Toole and L. L. Leung, The single-stranded DNA aptamer-binding site of human thrombin, *J. Biol. Chem.*, 1993, **268**(28), 20808–20811, DOI: 10.1016/S0021-9258(19)36856-5.

4 H. Yang, Y. Zhou and J. Liu, G-quadruplex DNA for construction of biosensors, *TrAC Trends in Analytical Chemistry*, 2020, **132**, 116060, DOI: 10.1016/j.trac.2020.116060; S. Wang, Construction of DNA Biosensors for Mercury (II) Ion Detection Based on Enzyme-Driven Signal Amplification Strategy, *Biomolecules*, 2021, **11**(3), 399; F. Wang, Y. Zhang, M. Lu, Y. Du, M. Chen, S. Meng, W. Ji, C. Sun and W. Peng, Near-infrared band Gold nanoparticles-Au film "hot spot" model based label-free ultratrace lead (II) ions detection via fiber SPR DNAzyme biosensor, *Sens. Actuators, B*, 2021, **337**, 129816, DOI: 10.1016/j.snb.2021.129816.

5 H. Du, C. M. Strohsahl, J. Camera, B. L. Miller and T. D. Krauss, Sensitivity and Specificity of Metal Surface-Immobilized "Molecular Beacon" Biosensors, *J. Am. Chem. Soc.*, 2005, **127**(21), 7932–7940, DOI: 10.1021/ja042482a; A. Liu, K. Wang, S. Weng, Y. Lei, L. Lin, W. Chen, X. Lin and Y. Chen, Development of electrochemical DNA biosensors, *TrAC, Trends Anal. Chem.*, 2012, **37**, 101–111, DOI: 10.1016/j.trac.2012.03.008; H. Du, M. D. Disney, B. L. Miller and T. D. Krauss, Hybridization-Based Unquenching of DNA Hairpins on Au Surfaces: Prototypical "Molecular Beacon" Biosensors, *J. Am. Chem. Soc.*, 2003, **125**(14), 4012–4013, DOI: 10.1021/ja0290781.

6 Y. Hua, J. Ma, D. Li and R. Wang, DNA-Based Biosensors for the Biochemical Analysis: A Review, *Biosensors*, 2022, **12**(3), 183.

7 J. R. Hutton, Renaturation kinetics and thermal stability of DNA in aqueous solutions of formamide and urea, *Nucleic Acids Res.*, 1977, **4**(10), 3537–3555; R. Blake and S. G. Delcourt, Thermal stability of DNA, *Nucleic Acids Res.*, 1998, **26**(14), 3323–3332.

8 J. Wang, Survey and summary: From DNA biosensors to gene chips, *Nucleic Acids Res.*, 2000, **28**(16), 3011–3016.

9 J.-W. Keum and H. Bermudez, Enhanced resistance of DNA nanostructures to enzymatic digestion, *Chem. Commun.*, 2009, (45), 7036–7038; C. Xue, S. Zhang, X. Yu, S. Hu, Y. Lu and Z. S. Wu, Periodically ordered, nuclease-resistant DNA nanowires decorated with cell-specific aptamers as selective theranostic agents, *Angew. Chem.*, 2020, **132**(40), 17693–17700.

10 J. Canoura, H. Yu, O. Alkhamis, D. Roncancio, R. Farhana and Y. Xiao, Accelerating post-SELEX aptamer engineering using exonuclease digestion, *J Am. Chem. Soc.*, 2020, **143**(2), 805–816; Z. Zhuo, Y. Yu, M. Wang, J. Li, Z. Zhang, J. Liu, X. Wu, A. Lu, G. Zhang and B. Zhang, Recent advances in SELEX technology and aptamer applications in biomedicine, *Int. J. Mol. Sci.*, 2017, **18**(10), 2142.

11 H. Qu, C. Fan, M. Chen, X. Zhang, Q. Yan, Y. Wang, S. Zhang, Z. Gong, L. Shi and X. Li, Recent advances of fluorescent biosensors based on cyclic signal amplification technology in biomedical detection, *J. Nanobiotechnol.*, 2021, **19**(1), 403.

12 P. Kim, M. Y. Choi, Y. Lee, K.-B. Lee and J.-H. Choi, Multiplexed Optical Nanobiosensing Technologies for Disease Biomarker Detection, *Biosensors*, 2025, **15**(10), 682.

13 K. Ettayri, Z. Gu, H. Yang, Y. Chen, M. Ma, C. Wang, L. Long, K. Wang and J. Qian, Recent advances in DNA aptamer-based fluorescence biosensors from design strategies to diverse applications and future challenges: A review, *Int. J. Biol. Macromol.*, 2025, **327**, 147398, DOI: 10.1016/j.ijbiomac.2025.147398.

14 Y. Li, R. Su, H. Li, J. Guo, N. Hildebrandt and C. Sun, Fluorescent Aptasensors: Design Strategies and Applications in Analyzing Chemical Contamination of Food, *Anal. Chem.*,

Open Access Article. Published on 26 March 2026. Downloaded on 4/16/2026 1:26:30 AM. This article is licensed under a Creative Commons Attribution 3.0 Unported Licence.

2022, **94**(1), 193–224, DOI: 10.1021/acs.analchem.1c04294; Y. Zhou, C. Mahapatra, H. Chen, X. Peng, S. Ramakrishna and H. S. Nanda, Recent developments in fluorescent aptasensors for detection of antibiotics, *Curr. Opin. Biomed. Eng.*, 2020, **13**, 16–24, DOI: 10.1016/j.cobme.2019.08.003.

15 M. Bauch, K. Toma, M. Toma, Q. Zhang and J. Dostalek, Plasmon-Enhanced Fluorescence Biosensors: a Review, *Plasmonics*, 2014, **9**(4), 781–799, DOI: 10.1007/s11468-013-9660-5.

16 Z. Zhu, P. Yuan, S. Li, M. Garai, M. Hong and Q.-H. Xu, Plasmon-Enhanced Fluorescence in Coupled Nanostructures and Applications in DNA Detection, *ACS Appl. Bio Mater.*, 2018, **1**(1), 118–124, DOI: 10.1021/acsabm.8b00032; J.-F. Li, C.-Y. Li and R. F. Aroca, Plasmon-enhanced fluorescence spectroscopy, *Chemical Society Reviews*, 2017, **46**(13), 3962–3979, DOI: 10.1039/C7CS00169J; D. C. Mor, G. Aktug, K. Schmidt, P. Asokan, N. Asai, C.-J. Huang and J. Dostalek, Plasmon-enhanced fluorescence (bio)sensors and other bioanalytical technologies, *TrAC, Trends Anal. Chem.*, 2025, **183**, 118060, DOI: 10.1016/j.trac.2024.118060.

17 E. Kume, G. Almohammadi, D. Duleba, A. F. M Alotaibi, R. Gan, K. Mamaeva, A. L. Bradley, R. P. Johnson and J. H. Rice, Piezoelectric-Driven Amplification of Plasmon-Enhanced Fluorescence for Advanced Sensing Applications, *ACS Appl. Mater. Interfaces*, 2025, **17**(19), 28881–28893, DOI: 10.1021/acsami.5c03428.

18 H. Shaik, S. N. Rachith, K. J. Rudresh, A. S. Sheik, K. H. Thulasi Raman, P. Kondaiah and G. Mohan Rao, Towards β-phase formation probability in spin coated PVDF thin films, *J. Polym. Res.*, 2017, **24**(3), 35, DOI: 10.1007/s10965-017-1191-x.

19 H. Shaik, S. N. Rachith, K. J. Rudresh, A. S. Sheik, K. H. Thulasi Raman, P. Kondaiah and G. Mohan Rao, Towards β-phase formation probability in spin coated PVDF thin films, *J. Polym. Res.*, 2017, **24**, 1–6.

20 C. M. Costa, V. F. Cardoso, P. Martins, D. M. Correia, R. Gonçalves, P. Costa, V. Correia, C. Ribeiro, M. M. Fernandes and P. M. Martins, *et al.*, Smart and Multifunctional Materials Based on Electroactive Poly(vinylidene fluoride): Recent Advances and Opportunities in Sensors, Actuators, Energy, Environmental, and Biomedical Applications, *Chem. Rev.*, 2023, **123**(19), 11392–11487, DOI: 10.1021/acs.chemrev.3c00196.

21 Z. He, F. Rault, M. Lewandowski, E. Mohsenzadeh and F. Salaün, Electrospun PVDF Nanofibers for Piezoelectric Applications: A Review of the Influence of Electrospinning Parameters on the β Phase and Crystallinity Enhancement, *Polymers*, 2021, **13**(2), 174, DOI: 10.3390/polym13020174.

22 C. M. Costa, V. F. Cardoso, P. Martins, D. M. Correia, R. Gonçalves, P. Costa, V. Correia, C. Ribeiro, M. M. Fernandes and P. M. Martins, *et al.*, Smart and Multifunctional Materials Based on Electroactive Poly(vinylidene fluoride): Recent Advances and Opportunities in Sensors, Actuators, Energy, Environmental, and Biomedical Applications, *Chem. Rev.*, 2023, **123**(19), 11392–11487, DOI: 10.1021/acs.chemrev.3c00196.

23 S. Almohammed, S. Fedele, B. J. Rodriguez and J. H. Rice, Aligned diphenylalanine nanotube–silver nanoparticle templates for high-sensitivity surface-enhanced Raman scattering, *J. Raman Spectrosc.*, 2017, **48**(12), 1799–1807, DOI: 10.1002/jrs.5254.

24 J. Truong, A. Stoner, M. R. C. Sytu, T. R. Tatlock, D. H. Cho and J. I. Hahm, Elucidation of Strain-Dependent, Zinc Oxide Nanorod Response for Nanorod-Guided Fluorescence Intensity, *Nanomaterials*, 2022, **12**(20), 3558, DOI: 10.3390/nano12203558 From NLMX. Zhang, Y. Qiu, D. Yang, B. Li, H. Zhang and L. Hu, Enhancing performance of Ag–ZnO–Ag UV photodetector by piezo-phototronic effect, *RSC Adv.*, 2018, **8**(28), 15290–15296, DOI: 10.1039/C8RA01189C; M. R. C. Sytu, A. Stoner and J. I. Hahm, Strain-Modulated and Nanorod-Waveguided Fluorescence in Single Zinc Oxide Nanorod-Based Immunodetection, *Biosensors*, 2024, **14**(2), 85, DOI: 10.3390/bios14020085 From NLMQ. Yang, W. Wang, S. Xu and Z. L. Wang, Enhancing Light Emission of ZnO Microwire-Based Diodes by Piezo-Phototronic Effect, *Nano Lett.*, 2011, **11**(9), 4012–4017, DOI: 10.1021/nl202619d; S. Mohammadpourfazeli, S. Arash, A. Ansari, S. Yang, K. Mallick and R. Bagherzadeh, Future prospects and recent developments of polyvinylidene fluoride (PVDF) piezoelectric polymer; fabrication methods, structure, and electromechanical properties, *RSC Adv.*, 2022, **13**(1), 370–387, DOI: 10.1039/d2ra06774a.

25 N. Shehata, R. Nair, A. Jain, M. Gamal, A. Hassanin, S. Noman, I. Shyha, K. Kruczała, M. Saad and I. Kandas, Multifaceted enhancement of piezoelectricity and optical fluorescence in electrospun PVDF-ceria nanocomposite, *Sci. Rep.*, 2025, **15**(1), 14073, DOI: 10.1038/s41598-025-98048-2.

26 A. F. Alotaibi, W. A. Wani, G. Almohammadi, B. J. Rodriguez and J. H. Rice, Nanoimprinted PVDF–MWCNT Composites with Silver Coating as a Label-Free Plasmonic Platform for Ultrasensitive Detection, *ACS Appl. Nano Mater.*, 2025, **8**(15), 7440–7448, DOI: 10.1021/acsanm.4c06987; A. F. Alotaibi, R. Gan, E. Kume, D. Duleba, A. Alanazi, A. Finlay, R. P. Johnson and J. H. Rice, Flexible nanoimprinted substrate integrating piezoelectric potential and photonic-plasmonic resonances, *Nanoscale Adv.*, 2025, **7**(8), 2360–2367, DOI: 10.1039/D4NA00942H.

27 M. Harsha Vardhan Reddy, R. M. Al-Shammari, N. Al-Attar, E. Kennedy, L. Rogers, S. Lopez, M. O. Senge, T. E. Keyes and J. H. Rice, Micro- or nanorod and nanosphere structures derived from a series of phenyl-porphyrins, *Phys. Chem. Chem. Phys.*, 2014, **16**(9), 4386–4393, DOI: 10.1039/C3CP54936D.

28 G. Rosenblatt, B. Simkhovich, G. Bartal and M. Orenstein, Nonmodal Plasmonics: Controlling the Forced Optical Response of Nanostructures, *Phys. Rev. X*, 2020, **10**(1), 011071, DOI: 10.1103/PhysRevX.10.011071.

29 Y. Wei, L. Li, D. Sun, Y. Zhu and G. Tian, The effect of silica shell on the surface enhanced Raman scattering and fluorescence with Ag nanoparticles: A three-dimensional finite element method investigation, *Opt. Commun.*, 2018, **427**, 426–432, DOI: 10.1016/j.optcom.2018.06.086.

30 P. Viswanath and M. Yoshimura, Light-induced reversible phase transition in polyvinylidene fluoride-based nanocomposites, *SN Appl. Sci.*, 2019, **1**(11), 1519, DOI: 10.1007/s42452-019-1564-3.

31 J.-f Li, C.-Y. Li and R. F. Aroca, Plasmon-enhanced fluorescence spectroscopy, *Chem. Soc. Rev.*, 2017, **46**(13), 3962–3979.
32 J. Movilli, R. W. Kolkman, A. Rozzi, R. Corradini, L. I. Segerink and J. Huskens, Increasing the Sensitivity of Electrochemical DNA Detection by a Micropillar-Structured Biosensing Surface, *Langmuir*, 2020, **36**(16), 4272–4279, DOI: 10.1021/acs.langmuir.0c00144 From NLMX. Bin, E. H. Sargent and S. O. Kelley, Nanostructuring of Sensors Determines the Efficiency of Biomolecular Capture, *Anal. Chem.*, 2010, **82**(14), 5928–5931, DOI: 10.1021/ac101164n.

Open Access Article. Published on 26 March 2026. Downloaded on 4/16/2026 1:26:30 AM.
This article is licensed under a Creative Commons Attribution 3.0 Unported Licence.

This journal is © the Owner Societies 2026